A Flash-Lidar for In-Orbit Servicing

1st Anders H. Hansen
SINTEF Digital
Oslo, Norway

2nd Vincent Dubanchet
Thales Alenia Space
Cannes, France

3rd Trine Kirkhus
SINTEF Digital
Oslo, Norway

4th Karl Henrik Haugholt
SINTEF Digital
Oslo, Norway

Abstract—We present a novel flash-lidar method with applications in rendezvous, satellite servicing, and debris removal. The method has been realized as a functional breadboard model. A first-principles simulation tool has been developed, which accurately reproduces the novel features of the flash-lidar model. We correlate the performance of the model with the requirements of rendezvous and docking operations in a robotic in-orbit servicing mission, and compare with a novel structured light 3D camera also developed for space. In estimating trajectories for a docking scenario we get 1cm error in the position estimates.

Index Terms—Space, flash-LIDAR, Rendezvous, Servicing

I. INTRODUCTION

There is a growing interest in flash-lidar for space missions, ranging from precision rendezvous [1] and in-orbit servicing [2], [3] to landing operations [4]–[6]. Flash-lidars have several advantages over scanning lidars: low weight and volume, high frame rate, and no moving parts. A flash-lidar uses an image sensor for simultaneous 3D measurement of the whole scene. This leads to high pointing accuracy and low motion distortion, enabling efficient use of 3D data in robotic operations and navigation [7]. We present here the results so far from the development of a versatile flash-lidar for in-orbit servicing.

II. THE FLExM FLASH-LIDAR

The FLExM (Flash Lidar for Exploration Missions) instrument is based on architecture, hardware and machine vision tools of the UTOFIA underwater camera [8] which was developed in the EU H2020 project with the same name [9]. A breadboard-level precursor to FLExM was presented in [1].

A. CMOS-based LIDAR

Single-photon avalanche detector (SPAD) arrays are widely considered for flash-lidar in space and elsewhere (E.g. [2], [3], [5], [10]). A disadvantage of such sensors is their low dynamic range, susceptibility to stray light interference, and low fill factor [11].

FLExM, in contrast, uses a CMOS image sensor based on mass-market manufacturing. CMOS sensors can easily achieve megapixel resolution, which SPADs have only recently achieved [11], [12]. Fill factor can be close to 100% with back-side illumination. Importantly, CMOS technology benefits from mass-market design tools, supply chains and quality assurance.

The FLExM sensor utilizes a 6T pixel architecture that is optimized for timing accuracy. This, paired with a low-jitter,
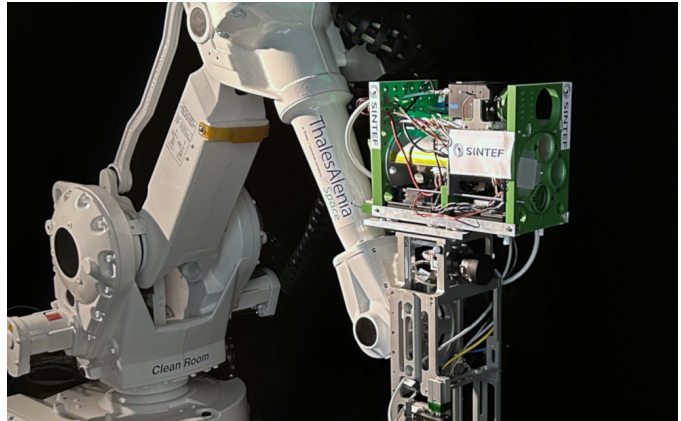
Fig. 1. FLExM breadboard model mounted on ROBY platform at Thales Alenia's robotics laboratory.

nanosecond-pulsed laser [13], enables efficient range-gating operation for 3D rendering.

B. Range-gated 3D

To obtain time-of-flight measurements, we employ *range-gating*: a method where the sensitivity of the receiver is sharply turned on (gated) a time Δt after the flash is emitted. In this way, light is only captured by the camera if its elapsed round-trip is greater than $c\Delta t$, leading to a dark foreground and a bright background separated by a range-gate at distance $c\Delta t/2$.

Our method, and the associated 3D algorithms, are described in detail in [8], where we also report on centimetre-level depth performance. Hardware-embedded algorithms provide fast reconstruction for real-time 3D video.

To meet the requirements of applicable space missions, the UTOFIA method has been modified and improved. Range-gating sequence control is adapted to long-range operation, with a search-and-detect mode for identifying distant targets. Data acquisition and pre-filtering has been optimized for low-light conditions. Signal processing is modified to meet spatial resolution targets. The optical delivery system is completely redesigned for above-water duty and to meet mission requirements.

III. TARGETED MISSIONS

FLExM is a versatile flash-lidar, intended for a variety of space applications with only minor hardware adjustments. We highlight here two applications that are being investigated

in detail in ongoing projects, and discuss the associated requirements for a supporting lidar system.

A. In-Orbit Servicing: EROSS IOD

EROSS is a planned in-orbit demonstration of autonomous rendezvous, docking and servicing of communication satellites. Mission design is ongoing through the EROSS EU Horizon projects[1][2]. 3D data from the flash-lidar will be of use throughout the mission to feed the Guidance, Navigation & Control (GNC) filters estimating the relative states of the Client vehicle on-board a Servicer vehicle..

The flash-lidar will make initial visual contact at $1-2$ km range, after which position and velocity measurements are sent to GNC for relative navigation. At ~100 m range, the servicer places itself in synchronous orbit and the flash-lidar performs 360-degree visual inspection of the client for damage inspection and pose estimation. In a final approach and docking stage, the flash-lidar identifies and tracks the contact point and transfers information to the robotic gripper. This visual servoing function is also applicable to subsequent servicing operations, such as refueling or payload replacement.

The time scale of each phase is largely determined by the orbital period of the client satellite. In geosynchronous orbit, a rendezvous may last several days. A flash-lidar can therefore be designed to perform slow measurements at low power, e.g. by reducing the laser pulse repetition rate.

B. Lunar Landing: Argonaut

The Argonaut (or *European Large Logistic Lander,* EL3) is a Lunar landing vehicle planned by ESA. Whereas the Apollo missions chose low-risk landing sites such as crater basins, the Argonaut must be able to land in more challenging areas such as the Lunar polar regions. This necessitates high-resolution, in-flight 3D vision to detect boulders and other hazards that cannot be mapped from orbit.

The associated requirements are far more challenging than in orbit, due to the short time allocation, wide target area, and need for advanced motion compensation. The flash-lidar will have to operate at peak efficiency to deliver a single 3D map within a $3-5$ second time window.

Flash-lidar is considered an attractive technology due to its mechanical robustness, high resolution and very high data rate. FLExM is one of several candidate lidar technologies in development for the Argonaut.

C. Mission Requirements

Table I lists the key requirements for a lidar system in the various operations discussed above. The in-orbit servicing mission is broken into three use cases as previously described, whereas the Lunar landing mission constitutes a single use case.

The list of requirements has been compiled from a variety of sources that the authors have access to, including confidential communications. Therefore, detailed source information
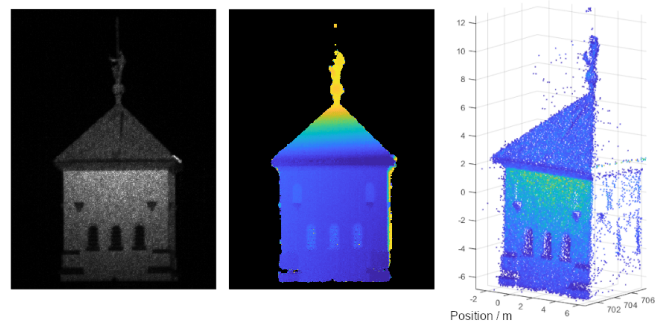
Fig. 2. Belltower from 700m range. Left: intensity image. Center: Depth image. Right: Point cloud representation.

cannot be provided. Where mission requirements are undetermined, reasonable approximate values have been used, for instance based on requirements from similar missions.

IV. TEST METHODOLOGY

Using the demonstrator model developed in [1], we have carried out functional and performance tests to correlate the system with mission requirements.

A. Long-range 3D rendering

Testing at kilometer-range is done using local bell towers as subjects. We have obtained 3D images at up to 4 km range. Fig. 2 shows the obtained 3D data of Ris Church in Oslo from 700 m range. For public safety reasons, the laser beam was baffled so that only the top of the belltower is sampled.

For these tests, the flash-lidar was equipped with a 135 mm f/2 camera objective. A holographic laser beam expander provided an approximately Gaussian beam with 1.5 degrees FWHM(full width at half maximum) expansion. Data was accumulated over 68 s to improve signal-to-noise statistics, with range-gating performed on the accumulated and averaged sensor data.

Due to weather conditions, we expect that a $3-6$ dB attenuation was present due to atmospheric scattering.

Additional long-range tests were performed on artificial, spherical targets. In these tests, we were easily able to resolve and detect a 12 cm target at 1 km range.

B. Close-range visual servoing

Flash-lidar data for more space-relevant targets was captured at the ROBY test facility at Thales Alenia Space in Cannes, France (Fig. 1). With this test bench, we were able to test the flash-lidar with complex, moving targets in an environment with controlled ambient light; however, working range was naturally limited by the size of the facility.

The ROBY test bench relies on the combination of an offline bench calibration with laser tracker systems, with online live measurements through industrial robot sensors and a motion capture system at the ceiling. The experimental data post-processing yields measurements with better than 1mm accuracy, potentially 0.3mm with proper calibration of the mockup 3D shape and with sensor extrinsic calibration. This ground

TABLE I
MISSION REQUIREMENTS

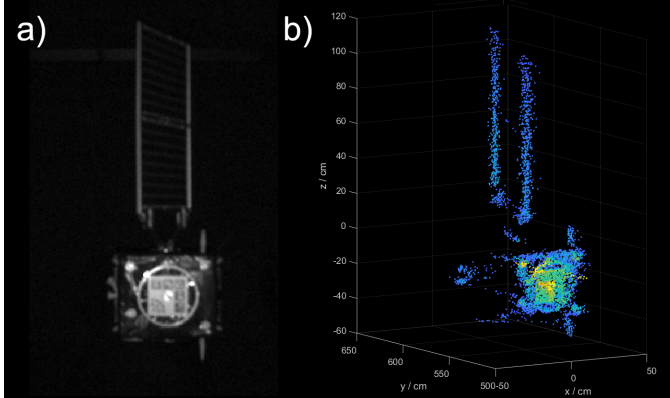|	In-Orbit Detection	In-Orbit Inspection	In-Orbit Approach	Lunar landing
Working range	2000 m	100 m	10 m	300 − 400 m
Duration	Hours	45 min − 12 hr	∼ 10 min	5 s
3D frame rate	0.1 Hz	1 Hz	5 Hz	0.2 Hz
Field of view	$1 - 2°$	$10°$	$30°$	$15°$
Sampling density	1 m	1 cm	1 mm	10 cm
	$0.03°$	$0.005°$	$0.005°$	$0.015°$
Point-wise ranging accuracy	1 %	1 cm	1 mm	10 cm

Fig. 3. Tracking of satellite mockup. a) Single camera frame (intensity image). b) 3D point cloud.

truth is taken as reference to evaluate the absolute performance of the flash-lidar along an approach trajectory from 10m down to 1m with lateral and depth motion combined.

3D data was captured for different dummy objects, which were constructed from space-relevant materials. The ROBY test bench provided robotic motion, with ground truth trajectory data to test against the lidar tracking data. Ground truth trajectories was given by the positioning system available at the ROBY test bench.

For this experiment, a 25 mm camera lens and wide-angle beam expander provided a 50-degree field-of-view. To prevent excessive signal levels, the camera lens was stopped to f/4. A frame rate of 1.6 Hz was used. Frame rates up to 50 Hz were eschewed in favor of using the (slow) raw data channel for off-line analysis.

The flash-lidar was configured to perform a 2m deep range sweep, with an adjustable offset. To map the whole trajectory of a target (2 − 12 meters), data from four identical test runs, each with a different sweep offset, were merged to one data set.

Tracking was performed in two ways: sequential point cloud registration, and fitting to a 3D model. This hybrid approach gives both absolute position and relative motion, and is thus appropriate for Kalman-filtering to improve accuracy. The 3D CAD model was an 8x8x8cm aluminum cube with matte, glass-blasted faces. A 1:3-scale mock-up satellite was used

for sequential point cloud registration (Fig. 3).

An Iterative Closest Point algorithm [14] was used for sequential tracking, which yields a step-wise rigid transformation from frame to frame. All analysis was performed in MATLAB, with high-level functions provided by the Computer Vision Toolbox.

Since we did not have an accurate calibration of the LIDAR pose relative to the test bench, we fitted the trajectory estimated from the sequential tracking with the ground truth using rigid 3D transforms. The error of individual trajectory point measurements was estimated from the root-mean-squared Euclidean residual of the best-fit, using the closest point-to-point distances.

V. TEST RESULTS

A. 3D mapping

The sampling density of the belltower is 7 cm, determined by the range and by choice of camera objective. Ranging precision was measured to be 5 cm by fitting a plane by least-squares to the front-facing wall. Due to lower reflectivity, the roof was less precisely resolved, by a factor consistent with a statistical square-root law.

The obtained accuracy is consistent with the requirements in Table I, provided some simple assumptions about range-scaling. In the figure, note the detailed reconstruction of the spire ornament. This level of performance is sufficient to resolve details on a satellite, such as control thrusters.

However, the acquisition time of 68 seconds is too long, even when correcting for atmospheric attenuation. The long acquisition is driven by the image sensor's poor noise characteristics. As we shall discuss in Section VIII, we are in the process of addressing this shortcoming.

B. Object tracking

The four lidar trajectories have been plotted in Fig. 4 together with the ground truth trajectory from the test bench. Visually, it is clear that we are achieving good tracking performance.

The accuracy of the sequential estimation is ∼1 cm. Although for a single point, the lateral accuracy is far greater than the longitudinal accuracy, the ICP method gives roughly isotropic error bars. Errors increase somewhat with distance due to signal scaling. Also, the nearest distances have increased errors due to non-linear effects near pixel saturation
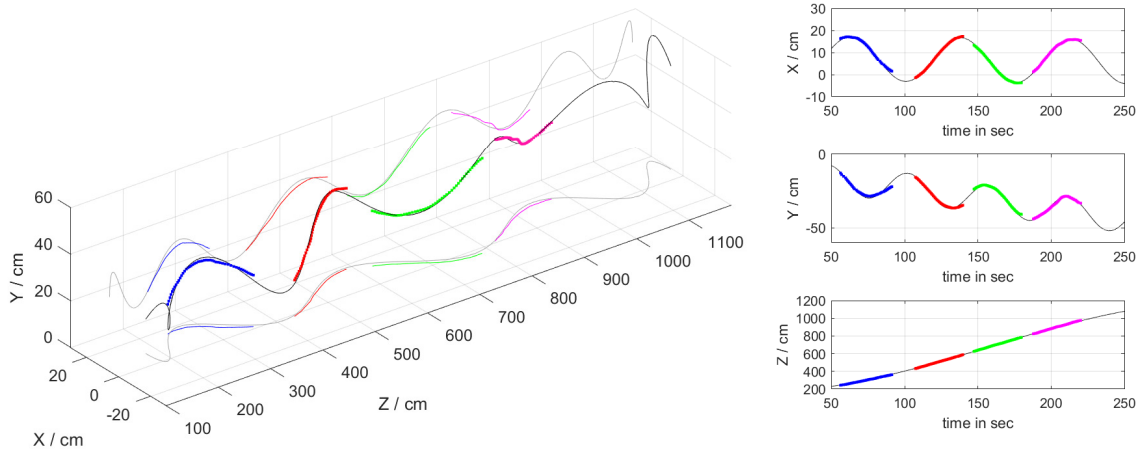
Fig. 4. Tracking of satellite trajectory. Black line is ground truth data; colored lines represent four data sets with different sweep offsets. On left is 3D plot of trajectory; projections are shown on xz- and xy planes. On right is a parametric representation of x, y and z-coordinates versus time.

– this despite our configuring the optics for short-range operation.

The 1 cm accuracy is good enough for all but the final stages of rendezvous and docking, when robotic and capture operations are at stake. In the final approach, several seconds of data must be Kalman-filtered to obtain the required 1 mm accuracy. An alternative that we have not explored, is to use the intensity images (Fig 3a) for 2D recognition; this reduces the dimensionality of the point cloud tracking, from low-precision 3D fitting to highly accurate 1D ranging.

VI. SIMULATION TOOL

There are currently no established tools for simulating a range-gated flash-lidar. We have therefore developed our own simulation tool from scratch. The simulator uses, in many cases, first-principles physics to account for subtle, but crucial characteristics such as electron transport properties of the camera pixel, which determines the shape of the exposure gate.

The simulator is implemented in MATLAB, with additional functionality imported from the PyVista visualization library. The core of the simulator is implemented in four logic blocks (Fig. 5): 1) a renderer that loads a CAD-model of the target and computes target range and reflectivity for each camera pixel; 2) a radiometric calculator that counts the expected number of photons per pixel; 3) a range-gating simulator that implements pixel dynamics; and 4) and a noise renderer that blends statistical shot noise with a buffer archive of real, recorded sensor dark noise. The output is a single, range-gated frame.

Batch operation of the simulator produces range-sweeps, which may be used to test the flash-lidar 3D algorithm. In this way, we can estimate the performance of the instrument under various space-like conditions.

A. Rendezvous Simulations

The simulator tool has been used to explore various rendezvous operations. These include deep-field detection and
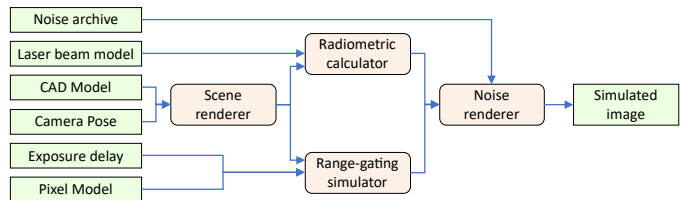

Fig. 5. Logic flow of simulator tool. Output is a single, range-gated frame.

ranging, object tracking, inspection, and final approach.

Using 3D models of the EROSS client satellite, we can explore docking scenarios, and experiment with different lidar configurations. The accuracy of the simulator has been validated by comparing simulated data with real data using the mock-up client (Fig. 6).
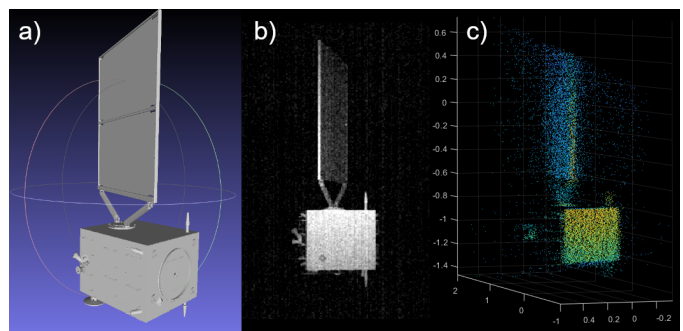

Fig. 6. Simulated satellite rendezvous, using model of satellite in Fig. 3. a) CAD model. b) Simulated camera frame (intensity). c) Point cloud reconstruction from simulated sensor data.

B. Moon Landing Simulations

The simulator can be run with relative motion between the instrument and target. This is needed to accurately simulate a Lunar landing scenario, where the lidar may be moving at > 100 km/h during operation. The simulator is a valuable tool

for validating new algorithms for motion compensation (Fig. 7) and testing accuracy of digital elevation map rendering.

We have developed a library of 3D models of landing sites, including realistic Lunar terrain and various "dummy" surfaces with e.g. rocks and boulders included. Our results suggest that we can achieve 10x10x10 cm resolution from over 300m altitude when moving at 100km/h under realistic conditions. Hence we can reliably detect boulders less than 30 cm.
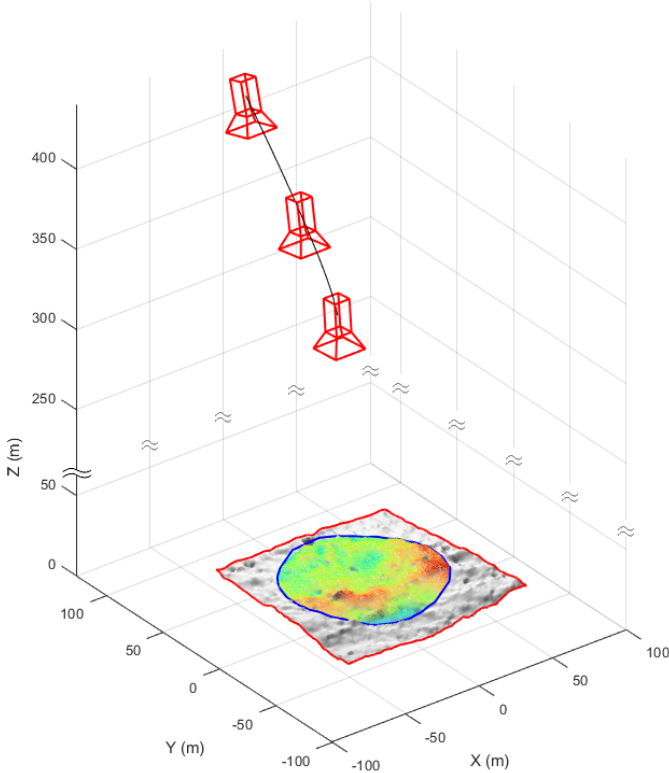

Fig. 7. Simulated Lunar landing. Data is acquired while in a curved trajectory between 400 and 300 m altitude, and a digital elevation map (false color) is reconstructed. Vertical axis compressed for visual clarity.

VII. 3D VISION FOR SPACE: IN PERSPECTIVE

Autonomous systems and robotics are becoming increasingly common, increasing the demand for advanced spatial perception in space. 3D vision systems can be broadly divided into time-of-flight (lidar) and epipolar (stereo, pattern projection) methods. Time-of-flight systems tend to be larger and less accurate, but are able to operate at much greater ranges. Epipolar systems are limited to $\sim$ 10x their baseline, but offer much greater resolution. A summary of selected space-relevant technologies is provided in Table II.

A successful rendezvous requires sensors that can operate from several km range down to less than 1 m. Although a flash-lidar can cover this whole range, its performance is outmatched by other technologies at the shortest distances. In the final approach to a client, very high accuracy is required to ensure a safe and successful coupling. Furthermore, a wide operational range requires dynamic attenuation of a lidar signal path, e.g.

by adjusting laser power or adjusting receiving optics - adding weight, complexity, or both.

At these shortest ranges, stereo vision generally achieves better 3D accuracy than time-of-flight methods [18], [19]. For this reason, SINTEF has developed a compact active-stereo camera with a road map toward space [16]. This camera features spatial resolutions of 0.1 mm in each dimension and 10 Hz measurement rates, with a size and weight that allows mounting on robotic arms, including the gripper arm.

A combination of long- and short-range technologies can offer high-quality 3D vision throughout a rendezvous and service operation. Such a hybrid 3D vision system would rely on the flash-LIDAR at ranges greater than a few meters, and, during final approach, transfer control from flash-lidar data to active-stereo data as the latter becomes more reliable.

VIII. PRESENT AND FUTURE WORK

A. Flash-lidar maturation

Several projects have been launched to elevate our hardware platform from its current technology readiness level (TRL) of 4 toward a space-ready product.

The most important bottleneck is the CMOS sensor, which is based on a design from 2001. Sensor designer Caeleste BV is collaborating to develop the space-grade *FLAMES* sensor that leverages 20 years of fabrication advancements to deliver up to 15 times greater signal-to-noise ratio. This will lead to better point cloud accuracy and higher frame rates. The current ESA-funded project aims to deliver by 2024 a TRL-5 FLAMES-sensor based on a TRL-6 chip design.

In parallel, the FLExM maturation project aims to deliver an updated breadboard model at TRL-5, including the new image sensor and an updated laser design with a target 2x increase in pulse energy. The project will perform de-risking of components, and propose a roadmap toward space. Finally, this project will correlate instrument specifications with Lunar landing missions, and propose a candidate flash-lidar model for the Argonaut program.

B. Simulator rendering

The 3D rendering block of the simulator architecture treats all surfaces as diffuse (Lambertian) with a single, global albedo. While this is a good approximation in the original Lunar surface use case, it is not at all accurate for satellites. Metal foils, solar panels and radiators have specular and/or highly absorptive optical properties that may affect flash-lidar performance. Furthermore, the current renderer cannot reproduce printed features. A comparison of Figs. 3 and 6 demonstrates the effects of this limitation.

An upgrade to the renderer is planned, where "colored" models can be loaded and interpreted with different surface properties. Improvements to the radiometric calculator block will interpret surface properties and account for surface texture and albedo in its geometric calculations.

TABLE II
Indicative Trade-Off Table Between Optical 3D Technologies

Technology	Working Range	Accuracy	Data Density	Sunlight Tolerance	Power	Size	Computational Load
Flash-lidar (ours) [1]	2 m – 4 km	Low	Dense	Good	High	Large	Medium
SPAD Flash-lidar [2], [3]	1 m – 300 m	Low	Dense	Bad	Medium	Large	High
Scanning lidar [15]	1 m – 1.5 km	Medium	Dense	Good	High	Very Large	Low
Structured Light [16]	0.5 m – 1.5 m	High	Dense	Good	Medium	Medium	High
Stereo, unassisted [17]	0.5 m – 1.5 m	Medium	Sparse	Very Good	Medium	Medium	High
2D vision with markers	0.5 m – 1.5 m	Medium	Very Sparse	Good	Low	Small	Medium

References

[1] K. H. Haugholt, A. H. Hansen, P. Risholm, J. T. Thielemann, and G. Tzeremes, "Development of A Flash-Lidar Elegant Breadboard Model for Rendezvous Applications," in *IGARSS 2020 - 2020 IEEE International Geoscience and Remote Sensing Symposium*. Waikoloa, HI, USA: IEEE, Sep. 2020, pp. 3483–3486.

[2] A. Pollini, C. Pache, and J. Haesler, "CSEM Space Lidars for Imaging and Rangefinding," in *IGARSS 2018 - 2018 IEEE International Geoscience and Remote Sensing Symposium*, Jul. 2018, pp. 1849–1852, iSSN: 2153-7003.

[3] G. Aglietti, B. Taylor, S. Fellowes, S. Ainley, D. Tye, C. Cox, A. Zarkesh, A. Mafficini, N. Vinkoff, K. Bashford, T. Salmon, I. Retat, C. Burgess, A. Hall, T. Chabot, K. Kanani, A. Pisseloup, C. Bernal, F. Chaumette, A. Pollini, and W. Steyn, "RemoveDEBRIS: An in-orbit demonstration of technologies for the removal of space debris," *The Aeronautical Journal*, vol. 124, no. 1271, pp. 1–23, Jan. 2020.

[4] F. Amzajerdian, A. Bulyshev, P. Brewster, G. Shen, J. Heppler, N. Dostart, and A. Gragossian, "Development of a 3-D Flash Lidar for Terrain Sensing and Safe Landing on Planetary Bodies," in *Optica Advanced Photonics Congress 2022*. Barcelona: Optica Publishing Group, 2022, p. LsM3C.2.

[5] M. Perenzoni, D. Perenzoni, and D. Stoppa, "A 64 $\times$ 64-Pixels Digital Silicon Photomultiplier Direct TOF Sensor With 100-MPhotons/s/pixel Background Rejection and Imaging/Altimeter Mode With 0.14% Precision Up To 6 km for Spacecraft Navigation and Landing," *IEEE Journal of Solid-State Circuits*, vol. 52, no. 1, pp. 151–160, Jan. 2017.

[6] A. E. Johnson, A. Huertas, R. A. Werner, and J. F. Montgomery, "Analysis of On-Board Hazard Detection and Avoidance for Safe Lunar Landing," in *2008 IEEE Aerospace Conference*, Mar. 2008, pp. 1–9, iSSN: 1095-323X.

[7] J. Pereira do Carmo, B. Moebius, M. Pfennigbauer, R. Bond, I. Bakalski, M. Foster, S. Bellis, M. Humphries, R. Fisackerly, and B. Houdou, "Imaging lidars for space applications," in *SPIE 7061, Novel Optical Systems Design and Optimization XI*, R. J. Koshel, G. G. Gregory, J. D. Moore, Jr., and D. H. Krevor, Eds., San Diego, California, USA, Aug. 2008, p. 70610J.

[8] P. Risholm, J. Thorstensen, J. T. Thielemann, K. Kaspersen, J. Tschudi, C. Yates, C. Softley, I. Abrosimov, J. Alexander, and K. H. Haugholt, "Real-time super-resolved 3D in turbid water using a fast range-gated CMOS camera," *Applied Optics*, vol. 57, no. 14, p. 3927, May 2018.

[9] J. T. Thielemann, "UTOFIA." [Online]. Available: https://cordis.europa.eu/project/id/633098

[10] F. Villa, F. Severini, F. Madonini, and F. Zappa, "SPADs and SiPMs Arrays for Long-Range High-Speed Light Detection and Ranging (LiDAR)," *Sensors*, vol. 21, no. 11, p. 3839, Jun. 2021.

[11] K. Morimoto, J. Iwata, M. Shinohara, H. Sekine, A. Abdelghafar, H. Tsuchiya, Y. Kuroda, K. Tojima, W. Endo, Y. Maehashi, Y. Ota, T. Sasago, S. Maekawa, S. Hikosaka, T. Kanou, A. Kato, T. Tezuka, S. Yoshizaki, T. Ogawa, K. Uehira, A. Ehara, F. Inui, Y. Matsuno, K. Sakurai, and T. Ichikawa, "3.2 Megapixel 3D-Stacked Charge Focusing SPAD for Low-Light Imaging and Depth Sensing," in *2021 IEEE International Electron Devices Meeting (IEDM)*. San Francisco, CA, USA: IEEE, Dec. 2021, pp. 20.2.1–20.2.4.

[12] A. C. Ulku, C. Bruschini, I. M. Antolovic, Y. Kuo, R. Ankri, S. Weiss, X. Michalet, and E. Charbon, "A 512 × 512 SPAD Image Sensor With Integrated Gating for Widefield FLIM," *IEEE Journal of Selected Topics in Quantum Electronics*, vol. 25, no. 1, pp. 1–12, Jan. 2019.

[13] E. Cametti, S. Dell'Acqua, P. Farinello, G. Piccinno, and G. Reali, "UTOFIA Project: A novel MOPA laser source for a compact, cost-effective system for underwater range-gated imaging," in *18th Italian National Conference on Photonic Technologies*, Jan. 2016, pp. 74 (4.)–74 (4.).

[14] A. Segal, D. Haehnel, and S. Thrun, "Generalized-ICP," in *Robotics: Science and Systems V*. Robotics: Science and Systems Foundation, Jun. 2009. [Online]. Available: http://www.roboticsproceedings.org/rss05/p21.pdf

[15] F. M. Kolb, M. Windmüller, M. Rößler, B. Möbius, P. Casiez, B. Cavrois, and O. Mongrard, "THE LIRIS-2 3D IMAGING LIDAR ON ATV-5," Breckenridge Colorado, USA, Feb. 2016, pp. 1023–1028.

[16] J. Thorstensen, J. T. Thielemann, P. Risholm, J. Gjessing, R. Dahl-Hansen, and J. Tschudi, "High-quality dense 3D point clouds with active stereo and a miniaturizable interferometric pattern projector," *Optics Express*, vol. 29, no. 25, pp. 41081–41097, Dec. 2021. [Online]. Available: https://www.osapublishing.org/oe/abstract.cfm?uri=oe-29-25-41081

[17] J. F. Bell, J. N. Maki, G. L. Mehall, M. A. Ravine, M. A. Caplinger, Z. J. Bailey, S. Brylow, J. A. Schaffner, K. M. Kinch, M. B. Madsen, A. Winhold, A. G. Hayes, P. Corlies, C. Tate, M. Barrington, E. Cisneros, E. Jensen, K. Paris, K. Crawford, C. Rojas, L. Mehall, J. Joseph, J. B. Proton, N. Cluff, R. G. Deen, B. Betts, E. Cloutis, A. J. Coates, A. Colaprete, K. S. Edgett, B. L. Ehlmann, S. Fagents, J. P. Grotzinger, C. Hardgrove, K. E. Herkenhoff, B. Horgan, R. Jaumann, J. R. Johnson, M. Lemmon, G. Paar, M. Caballo-Perucha, S. Gupta, C. Traxler, F. Preusker, M. S. Rice, M. S. Robinson, N. Schmitz, R. Sullivan, and M. J. Wolff, "The Mars 2020 Perseverance Rover Mast Camera Zoom (Mastcam-Z) Multispectral, Stereoscopic Imaging Investigation," *Space Science Reviews*, vol. 217, no. 1, p. 24, Feb. 2021. [Online]. Available: https://doi.org/10.1007/s11214-020-00755-x

[18] G. Bouquet, J. Thorstensen, K. A. H. Bakke, and P. Risholm, "Design tool for TOF and SL based 3D cameras," *Optics Express*, vol. 25, no. 22, pp. 27758–27769, Oct. 2017.

[19] Y. Liu, N. Pears, P. L. Rosin, and P. Huber, Eds., *3D Imaging, Analysis and Applications*. Cham: Springer International Publishing, 2020. [Online]. Available: http://link.springer.com/10.1007/978-3-030-44070-1